Letter | Editors' Suggestion

# Radiative Thermal Runaway Due to Negative-Differential Thermal Emission Across a Solid-Solid Phase Transition

David M. Bierman,[1] Andrej Lenert,[2] Mikhail A. Kats,[3] You Zhou,[5] Shuyan Zhang,[4] Matthew De La Ossa,[1] Shriram Ramanathan,[6] Federico Capasso,[4] and Evelyn N. Wang[1,*]

[1]*Department of Mechanical Engineering, Massachusetts Institute of Technology, Cambridge, Massachusetts 02139, USA*

[2]*Department of Chemical Engineering, University of Michigan, Ann Arbor, Michigan 48109, USA*

[3]*Department of Electrical and Computer Engineering, University of Wisconsin-Madison, Madison, Wisconsin 53706, USA*

[4]*John A. Paulson School of Engineering and Applied Sciences, Harvard University, Cambridge, Massachusetts 02139, USA*

[5]*Department of Chemistry and Chemical Biology, Harvard University, Cambridge, Massachusetts 02138, USA*

[6]*School of Materials Engineering, Purdue University, West Lafayette, Indiana 47907, USA*

(Received 13 December 2017; revised manuscript received 26 April 2018; published 3 August 2018)

Thermal runaway occurs when a rise in system temperature results in heat-generation rates exceeding dissipation rates. Here, we demonstrate that thermal runaway occurs in radiative (photon) systems given a sufficient level of negative-differential thermal emission. By exploiting the insulator-to-metal phase transition of vanadium dioxide, we show that a small increase in heat generation (e.g., 10 nW/mm$^2$) results in a large change in surface temperature (e.g., ∼35 K), as the thermal emitter switches from high emittance to low emittance. While thermal runaway is typically associated with catastrophic failure mechanisms, detailed understanding and control of this phenomenon may give rise to new opportunities in infrared sensing, camouflage, and rectification.

DOI: 10.1103/PhysRevApplied.10.021001

## I. INTRODUCTION

Thermal runaway is a positive feedback phenomenon that occurs when a rise in system temperature leads to a further increase in temperature. Such behavior has been observed in many different contexts, including exothermic chemical reactions [1,2], nuclear fusion reactions [3,4], self-heating in semiconductors [5,6], thermal (phonon) conduction [7–11], fluid boiling [12,13], and the greenhouse effect [14]. Here, we demonstrate and characterize the dynamics of thermal runaway in a radiative (photon) system. We show that thermal runaway is possible in a system where heat is dissipated from an emitter to the environment through far-field thermal radiation if the emitter exhibits a sufficient level of negative-differential emission (NDE)—decreasing emission with increasing temperature. A small increase in applied heat flux initiates strong NDE and results in a large change in temperature until NDE ceases and equilibrium is reestablished. We describe the necessary physical criteria to observe runaway (i.e., the required temperature coefficient of emittance) and its characteristic switching time. By minimizing the thermal mass of our emitters, we show that rapid (∼1 s) thermal switching is achievable, which is desirable for sensing applications.

In this work, runaway is enabled by the strong dependence of the optical properties of vanadium dioxide ($VO_2$) on temperature across its solid-solid phase transition, resulting in a temperature-dependent thermal emittance. $VO_2$ is a correlated-electron material that transitions from an insulator to a metal near room temperature (∼340 K) [15–17]. This transition is accompanied by a dramatic change in optical properties in the mid-infrared spectral range [16,18–22]. For example, thin films of $VO_2$ on sapphire exhibit a strong modulation of emittance across the phase transition [23]. Related concepts to thermal runaway such as bistability [24], thermal rectification [25–34], and thermal regulation or homeostasis [35] have been investigated in a variety of radiative systems. However, our work is the first experimental demonstration of thermal runaway in a radiative system. Thermal runaway, as demonstrated here, is also direct proof of the existence of broadband, hemispherical NDE in our geometry.

## II. CRITERIA FOR NDE

In a situation in which thermal radiation is the only form of heat transfer, the heat flux, defined as the heat loss per

*enwang@mit.edu

 

unit area, is well described by the Stefan-Boltzmann law [36],

$$Q(T) = \varepsilon(T)\sigma T^4, \tag{1}$$

where $Q$ is the radiative emissive power, $T$ is the temperature, $\varepsilon$ is the total spectrum- and angle-integrated emittance from a surface at a given $T$, and $\sigma$ is the Stefan-Boltzmann constant. The criterion for NDE can be determined by differentiating Eq. (1),

$$dQ(T)/dT = 4\varepsilon(T)\sigma T^3 + \sigma T^4 d\varepsilon(T)/dT. \tag{2}$$

For $Q$ to decrease with increasing $T$, and hence for NDE to be possible in the far field, the temperature coefficient of emittance (TCE), defined as

$$\mathrm{TCE} = \frac{1}{\varepsilon}\left|\frac{d\varepsilon(T)}{dT}\right|, \tag{3}$$

must meet the following criteria:

$$\mathrm{TCE} > \frac{4}{T}, \qquad \frac{d\varepsilon(T)}{dT} < 0. \tag{4}$$

The criterion for achieving NDE is less stringent at high temperatures. At lower temperatures, a higher value of TCE is required to observe NDE.

For $VO_2$, the phase transition occurs at ∼340 K. At this temperature, the TCE must be larger than ∼0.01 $K^{-1}$. We estimate that the TCE of demonstrated $VO_2$-based emitters is as large as 0.05 $K^{-1}$ [22], making this material a good candidate to study NDE and thermal runaway. It should be noted, however, that NDE can only be observed in a radiative (photon) system if radiation is the dominant heat-transfer mechanism, as discussed below.

## III. EXPERIMENTAL DEMONSTRATION

We grew an epitaxial $VO_2$ film (150 nm thick) on a 0.5-mm-thick polished single-crystal *c*-plane sapphire substrate using rf-magnetron sputtering from a $V_2O_5$ target (99.9% purity, AJA International Inc.). The substrate was held at 823 K during growth, with an rf-source-gun power of 125 W. Since the stoichiometry of $VO_2$ thin films is sensitive to the partial pressure of $O_2$ during the growth, the oxygen partial pressure was carefully tuned to optimize the resistivity change across the insulator-to-metal transition. In particular, we used a sputtering gas mixture composed of 99.50 sccm [cubic centimeters per minute at STP (standard temperature and pressure)] of Ar and 0.5 sccm of $O_2$ while keeping the chamber pressure at 10 mTorr. The deposited $VO_2$ films are epitaxial on *c*-plane sapphire with three orders of magnitude change in resistivity across the phase transition [37,38].

We designed a custom experiment to study how this sample behaves when a variable amount of radiative heat

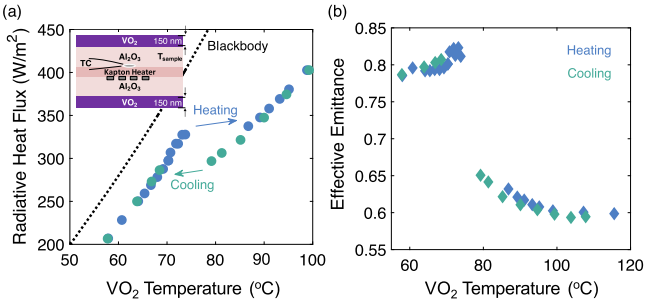


FIG. 1. (a) Steady-state heating and cooling characteristics of a thin-film $VO_2$ emitter structure, wherein the $VO_2$ film undergoes a temperature-driven insulator-to-metal transition. Note that the independent variable is the radiative heat flux (vertical axis). The thermal runaway is characterized by a ∼15 K jump in temperature, attributed to an abrupt reduction in the emittance of the surface. Also included is the calculated heat flux from a blackbody, for reference. Inset: Schematic of the emitting assembly, where the resistive heater is embedded between two slabs of sapphire, each coated with a $VO_2$ film on the outer surface. (b) Effective emittance of the assembly (i.e., the measured heat flux normalized by a theoretical blackbody).

flux is dissipated from its surface. The emitters were resistively heated with a heater sandwiched between two sapphire wafers. Thin-film $VO_2$ coats both polished external surfaces (Fig. 1 inset). Thermal conduction through the thermocouple and electrical leads is assumed to be negligible compared to the radiative emission (<5%, see Heat Transfer Model for details). Therefore, we assume that the electrical power dissipated in the device results in thermal radiation either from the $VO_2$ film or from the sides of the assembly.

The sample-heater-sample assembly was placed into a vacuum chamber in view of an infrared-transparent viewport, which was used for visualization of the runaway process with an infrared camera (sensitive to the 3–5-$\mu$m spectral range). The chamber was evacuated to 0.1 Pa, such that the heat loss by conduction from the heated surface was much smaller than that of the thermal radiation. Step changes in voltage were applied to the heater, and the time responses of the temperature and infrared signal were monitored. Data were recorded after an initial settling period, such that variations in the temperature measurement were within the uncertainty of the thermocouple (∼0.1 K).

Figure 1 shows the results of the experiment during the heating and cooling cycles. In Fig. 1(a), the sample temperature initially increases with electrical power delivered to the heater. However, at a heater power of ∼0.495 W (a total radiative heat flux of ∼330 W/m$^2$), the $VO_2$ film begins to change phase, resulting in NDE. Since the input power (i.e., dissipated power) remains constant, we observe thermal runaway until the structure reaches thermal equilibrium with $VO_2$ in its fully metallic state. The temperature increases by ∼15 °C because of

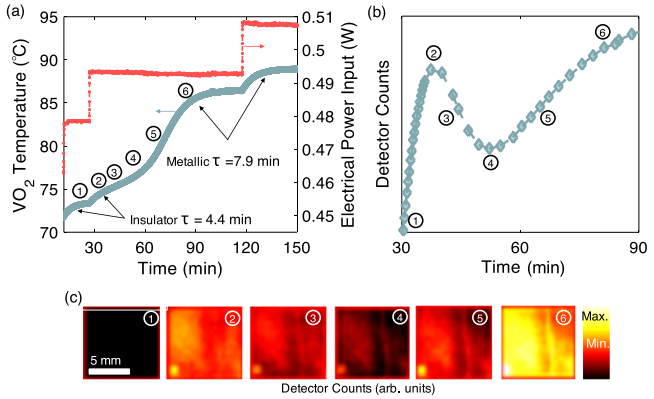


FIG. 2. Dynamics of thermal runaway: (a) $VO_2$ temperature (assumed to be equal to the assembly temperature based on a lumped thermal capacitance model) plotted as a function of time before, during, and after the $VO_2$ phase transition. The secondary axis shows the applied heater power dissipated through the structure. (b) Average infrared signal in the 3–5-$\mu$m range from one of the $VO_2$-coated surfaces during the transition. (c) Infrared images corresponding to states 1 through 6, as denoted in the figures.

the reduction in emittance. Upon cooling, we observe the reverse process wherein reducing the heat flux induces a runaway transition back to the insulating phase; these data are also included in Figs. 1(a) and 1(b), showing hysteresis between the heating and cooling cycle. The width of hysteresis can be controlled by modifying the microstructure of the thin films (such as the grain size and the defect concentration), as the nucleation energy which determines hysteresis depends on the microstructure of the thin films [39].

Figure 1(b) shows the effective emittance (i.e., the radiative heat flux normalized to that of a blackbody) for the sandwiched assembly. This represents a weighted average of the emitted flux between the inactive (sides, supports, etc.) and active ($VO_2$-coated surface) emission areas. The total emittance for heating exhibits an enhancement at ∼70 °C (due to an ultra-thin-film interference effect described in Ref. [19,23,40]), before an abrupt change as the $VO_2$ film becomes increasingly metallic over a ∼20 °C window, resulting in decreasing emittance. The data in Fig. 1(b) correspond to a TCE of approximately 0.014 $K^{-1}$ (averaged over the transition), which satisfies the criterion in Eq. (4).

Figure 2(a) shows the system time response before, during, and after the insulator-to-metal transition, as the input power is increased from 462 to 507 mW in steps of ∼15 mW (red points). At temperatures far below and far above the phase transition, the observed responses (blue curve) are characteristic of a first-order dynamic response. This response can be mathematically defined by a linear, first-order differential equation with a characteristic $RC$ time constant $\tau$, where the thermal resistance ($R$) is primarily due to radiation from the sample, and $C$ is the heat capacitance of the sample [41]. A single, constant value of $C$ captures the behavior across the phase transition because the thin $VO_2$ film accounts for a negligible fraction of the overall thermal capacitance. The same statement, however, cannot be made for $R$. While the $VO_2$ is in the insulator phase, a best-fit $RC$ time constant of 4.44 min is determined. The time constant remains unchanged as the input power is stepped from 478 to 493 mW, until the emittance begins to decrease sharply at (2). The radiative thermal resistance increases as the emittance decreases, leading to larger steady-state temperatures and time constants. After another increase in input power (from 493 to 507 mW), another time constant is observed, which is associated with the higher radiative thermal resistance of the system when the $VO_2$ is in the metallic state. Here, a time constant of 7.9 min is extracted by fitting data after the transition (from 493 to 507 mW). This represents a ∼59% longer time constant relative to the insulating phase, indicating the system dynamics are heavily influenced by emission from the $VO_2$-coated areas.

Qualitative data from infrared imaging in the 3–5-$\mu$m range during the heating experiment confirm that NDE is the cause of the thermal runaway [Fig. 2(b)]. A series of six infrared images, correspond to six data points in Fig. 2(c), show how the emissive power decreases as the temperature monotonically increases.

## IV. HEAT TRANSFER MODEL

To describe the dynamics of the experiment, we use a lumped thermal capacitance model based on empirical data for temperature-dependent emittance [23]:

$$C\frac{dT}{dt} = Q_{\text{in}} - \varepsilon_{\text{ia}}A_{\text{ia}}\sigma(T^4 - T_\infty^4) - \varepsilon_{\text{VO}_2}(T)A_{\text{VO}_2}\sigma(T^4 - T_\infty^4), \quad (5)$$

where $C$ is the heat capacity of the system (extracted from the $RC$ fit in the previous section), $T_\infty$ is the ambient temperature, $Q_{in}$ is the input heat (measured), $\varepsilon_{\text{ia}}$ is the emittance of the non-$VO_2$ surfaces (the subscripts ia and $VO_2$ stand for inactive and active areas, respectively), and $A$ is the area. The emittance of the inactive area is assumed to be unity since it is covered with thick Kapton tape [42]. The lumped thermal capacitance model assumes that the temperature of the $VO_2$ film is equal to the assembly temperature. The assumption is valid here because the radiative resistance between the emitter and the surroundings (∼0.15 $m^2\,K^1\,W^{-1}$, see Fig. 1) is much greater than the conductive resistance within the assembly (∼$10^{-4}$ $m^2\,K^1\,W^{-1}$, based on the thickness and thermal conductivity of the sapphire substrate).

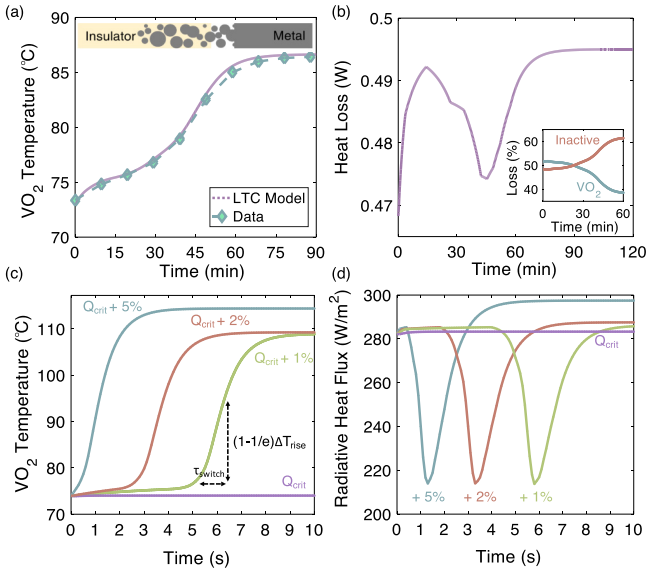


FIG. 3. Simulated thermal dynamics of our experimental assembly and an idealized thin-film assembly (sapphire thickness = 1 $\mu$m), demonstrating the limits and tunability of this thermal runaway process: (a) Time response of a lumped thermal capacitance with a temperature-dependent emittance that results from the percolation of the metallic phase. Experimental data are overlaid to show agreement. (b) Modeled transient heat loss from our device. Inset: percentage of heat loss from both the $VO_2$-covered and inactive surface areas. (c) Thermal runaway dynamics. With no overpotential above $Q''_{crit}$, the system equilibrates at 74 °C. By applying heat fluxes past this point, the onset of NDE can be modified. (d) The corresponding far-field radiative heat flux from the idealized device showing faster switching with increasing overpotential.

The results of this model agree with our experiments [Fig. 3(a)]. The model accurately predicts the time constants corresponding to the insulating and metallic phases of the device, as well as the steady-state temperatures. The total radiative heat loss of the system [Fig. 3(b)] highlights the nature of the NDE demonstrated in our experiment. Based on the optical properties of the system, a critical heat flux of ∼330 W m$^{-2}$ (∼0.49 W of the input power) is determined. This is the maximum possible radiative heat flux that can be supported by a surface with NDE properties without triggering thermal runaway. When the CHF is surpassed, $VO_2$ transitions to its metallic state before equilibrium can be established. As described by Eq. (4), this heat flow comprises both the active (from surfaces covered with $VO_2$) and inactive (from sides, leads, etc.) components [inset of Fig. 3(b)]. Heat loss through the inactive area attenuates the NDE phenomenon since these losses are not temperature dependent.

To investigate how quickly the emitter can switch given the optical properties of our thin-film $VO_2$ sample [Figs. 3(c) and 3(d)], we model an idealized thin-film assembly with a sapphire substrate thickness of 1 $\mu$m and no parasitic heat loss. This substrate thickness was chosen because it does not significantly affect the emittance properties [23]. At the CHF, the system is at equilibrium at 74 °C in an insulating phase, shown as a horizontal purple blue line in Fig. 3(c). An additional incremental flux is needed (e.g., 1% of CHF) to force the system to switch to its metallic state through the thermal runaway process. The total switching time in this case, defined as the time elapsed between the two equilibrium states, is approximately 10 s for a temperature rise of ∼35 °C. The characteristic exponential time constant ($\tau_{switch}$), equivalent to the *RC* time constant, is ∼1.5 s. A ∼5 s delay is observed before the NDE begins to trigger thermal runaway [Fig. 3(d)] which limits the overall switching speed. With higher "overpotentials", or percentages above the CHF (i.e., +5%), the delay becomes comparable to the characteristic switching time (∼1 s), improving the overall switching speed. Reducing the overall switching time below ∼1 s would require decreasing the *RC* time constant governed by the optical properties and thermal mass of the sapphire and metallic-phase $VO_2$ system. Since the characteristic time constant is limited by the thermal resistance of far-field radiation, near-field radiative transfer may be a potential approach to reduce the switching time.

Understanding the switching dynamics associated with radiative thermal runaway can enable the design of advanced thermal diodes, calorimeters, passive temperature control, and infrared sensors. For example, sensors can benefit from this characteristic sensitivity to small incremental fluxes near the CHF to resolve small-power signals. Whereas a 1 nW change in heat input raises the temperature by ∼1 °C of a 1 mm$^2$ isolated thin structure discussed above, a 1 nW additional flux near the CHF would trigger a thermal runaway and a much-larger change in temperature (∼35 °C).

## V. CONCLUSIONS

The concept of temperature-dependent emittance has a variety of applications, including passive temperature management [43], infrared camouflage [44], and remote sensing of small temperatures [45–47]. In this paper, we describe how the presence of sufficiently large negative-differential emittance can result in a thermal runaway process that can result in large temperature jumps in the emitter. We experimentally demonstrate this phenomenon using thermal emitters comprising phase-transition material vanadium dioxide ($VO_2$), and build corresponding models to better understand its dynamics. Though generally thermal runaway is associated with catastrophic-failure mechanisms, thermal runaway based on solid-solid phase transitions such as the one in $VO_2$ can be a robust and repeatable phenomenon, and can

thus be a component of dynamic thermal radiative systems.

## ACKNOWLEDGMENTS

This work is supported as part of the Solid-State Solar Thermal Energy Conversion (S3TEC) Center, an Energy Frontier Research Center funded by the U.S. Department of Energy, Office of Science, Office of Basic Energy Sciences under DE-FG02-09ER46577. M.A.K. acknowledges support from the Office of Naval Research (Grant No. N00014-16-1-2556). S.R. acknowledges support from Office of Naval Research (Grant No. N00014-16-1-2398).

[1] M. Morbidelli and A. Varma, A generalized criterion for parametric sensitivity: Application to thermal explosion theory, Chem. Eng. Sci. **43**, 91 (1988).
[2] J. C. Leung, H. K. Fauske, and H. G. Fisher, Thermal runaway reactions in a low thermal inertia apparatus, Thermochim. Acta **104**, 13 (1986).
[3] K. Nomoto, F.-K. Thielemann, and J. C. Wheeler, Explosive nucleosynthesis and Type I supernovae, Astrophys. J. **279**, L23 (1984).
[4] J. J. Cowan, A. G. W. Cameron, and J. W. Truran, The thermal runaway r-process, Astrophys. J. **252**, 348 (1982).
[5] V. M. Dwyer, A. J. Franklin, and D. S. Campbell, Thermal failure in semiconductor devices, Solid State Electron. **33**, 553 (1990).
[6] C. Popescu, Selfheating and thermal runaway phenomena in semiconductor devices, Solid State Electron. **13**, 441 (1970).
[7] W. Kobayashi, D. Sawaki, T. Omura, T. Katsufuji, Y. Moritomo, and I. Terasaki, Thermal rectification in the vicinity of a structural phase transition, Appl. Phys. Express **5**, 027302 (2012).
[8] B. Li, L. Wang, and G. Casati, Negative differential thermal resistance and thermal transistor, Appl. Phys. Lett. **88**, 143501 (2006).
[9] D. Sawaki, W. Kobayashi, Y. Moritomo, and I. Terasaki, Thermal rectification in bulk materials with asymmetric shape, Appl. Phys. Lett. **98**, 081915 (2011).
[10] C. W. Chang, D. Okawa, A. Majumdar, and A. Zettl, Solid-state thermal rectifier, Science **314**, 1121 (2006).
[11] W. Kobayashi, Y. Teraoka, and I. Terasaki, An oxide thermal rectifier, Appl. Phys. Lett. **95**, 171905 (2009).
[12] S. G. Kandlikar, A theoretical model to predict pool boiling CHF incorporating effects of contact angle and orientation, J. Heat Transf. **123**, 1071 (2001).
[13] T. G. Theofanous, T. N. Dinh, J. P. Tu, and A. T. Dinh, The boiling crisis phenomenon: Part II: dryout dynamics and burnout, Exp. Therm. Fluid Sci. **26**, 793 (2002).
[14] P. Friedlingstein, L. Bopp, P. Ciais, J.-L. Dufresne, L. Fairhead, H. LeTreut, P. Monfray, and J. Orr, Positive feedback between future climate change and the carbon cycle, Geophys. Res. Lett. **28**, 1543 (2001).
[15] M. Liu, H. Y. Hwang, H. Tao, A. C. Strikwerda, K. Fan, G. R. Keiser, A. J. Sternbach, K. G. West, S. Kittiwatanakul, J. Lu, S. A. Wolf, F. G. Omenetto, X. Zhang, K. A. Nelson, and R. D. Averitt, Terahertz-field-induced insulator-to-metal transition in vanadium dioxide metamaterial, Nature **487**, 345 (2012).
[16] A. Zylbersztejn and N. F. Mott, Metal-insulator transition in vanadium dioxide, Phys. Rev. B **11**, 4383 (1975).
[17] M. F. Jager, C. Ott, P. M. Kraus, C. J. Kaplan, W. Pouse, R. E. Marvel, R. F. Haglund, D. M. Neumark, and S. R. Leone, Tracking the insulator-to-metal phase transition in $VO_2$ with few-femtosecond extreme UV transient absorption spectroscopy, Proc. Natl. Acad. Sci. U. S. A. **114**, 9558 (2017).
[18] M. M. Qazilbash, M. Brehm, B.-G. Chae, P.-C. Ho, G. O. Andreev, B.-J. Kim, S. J. Yun, A. V. Balatsky, M. B. Maple, F. Keilmann, H.-T. Kim, and D. N. Basov, Mott transition in $VO_2$ revealed by infrared spectroscopy and nano-imaging, Science **318**, 1750 (2007).
[19] M. A. Kats, R. Blanchard, S. Ramanathan, and F. Capasso, Thin-film interference in lossy, ultra-thin layers, Opt. Photonics News **25**, 40 (2014).
[20] M. A. Kats, R. Blanchard, P. Genevet, Z. Yang, M. M. Qazilbash, D. N. Basov, S. Ramanathan, and F. Capasso, Thermal tuning of mid-infrared plasmonic antenna arrays using a phase change material, Opt. Lett. **38**, 368 (2013).
[21] M. A. Kats and F. Capasso, Optical absorbers based on strong interference in ultra-thin films, Laser Photon. Rev. **10**, 735 (2016).
[22] M. A. Kats, R. Blanchard, S. Zhang, P. Genevet, C. Ko, S. Ramanathan, and F. Capasso, Vanadium Dioxide as a Natural Disordered Metamaterial: Perfect Thermal Emission and Large Broadband Negative Differential Thermal Emittance, Phys. Rev. X **3**, 041004 (2013).
[23] M. A. Kats, D. Sharma, J. Lin, P. Genevet, R. Blanchard, Z. Yang, M. M. Qazilbash, D. N. Basov, S. Ramanathan, and F. Capasso, Ultra-thin perfect absorber employing a tunable phase change material, Appl. Phys. Lett. **101**, 221101 (2012).
[24] L. Zhu, C. R. Otey, and S. Fan, Negative differential thermal conductance through vacuum, Appl. Phys. Lett. **100**, 044104 (2012).
[25] A. Ghanekar, G. Xiao, and Y. Zheng, High contrast far-field radiative thermal diode, Sci. Rep. **7**, 6339 (2017).
[26] C. R. Otey, W. T. Lau, and S. Fan, Thermal rectification through vacuum, Phys. Rev. Lett. **104**, 154301 (2010).
[27] S. Basu and M. Francoeur, Near-field radiative transfer based thermal rectification using doped silicon, Appl. Phys. Lett. **98**, 113106 (2011).
[28] H. Iizuka and S. Fan, Rectification of evanescent heat transfer between dielectric-coated and uncoated silicon carbide plates, J. Appl. Phys. **112**, 024304 (2012).
[29] L. P. Wang and Z. M. Zhang, Thermal rectification enabled by near-field radiative heat transfer between intrinsic silicon and a dissimilar material, Nanoscale Microscale Thermophys. Eng. **17**, 337 (2013).
[30] L. Zhu, C. R. Otey, and S. Fan, Ultrahigh-contrast and large-bandwidth thermal rectification in near-field electromagnetic thermal transfer between nanoparticles, Phys. Rev. B **88**, 184301 (2013).
[31] P. Ben-Abdallah and S.-A. Biehs, Phase-change radiative thermal diode, Appl. Phys. Lett. **103**, 191907 (2013).

[32] Z. Chen, C. Wong, S. Lubner, S. Yee, J. Miller, W. Jang, C. Hardin, A. Fong, J. E. Garay, and C. Dames, A photon thermal diode, Nat. Commun. **5**, 5446 (2014).

[33] E. Nefzaoui, J. Drevillon, Y. Ezzahri, and K. Joulain, Simple far-field radiative thermal rectifier using Fabry–Perot cavities based infrared selective emitters, Appl. Opt. **53**, 3479 (2014).

[34] P. Ben-Abdallah and S.-A. Biehs, Near-Field Thermal Transistor, Phys. Rev. Lett. **112**, 044301 (2014).

[35] S.-H. Wu, M. Chen, L. Wang, M. Barako, V. Jankovic, P. Hon, L. Sweatlock, and M. Povinelli, in Conference on Lasers and Electro-Optics, 2017, p. SM3N.7.

[36] M. F. Modest, *Radiative Heat Transfer* (Elsevier Science, Oxford, UK, 2013).

[37] F. J. Wong, Y. Zhou, and S. Ramanathan, Epitaxial variants of $VO_2$ thin films on complex oxide single crystal substrates with 3 m surface symmetry, J. Cryst. Growth **364**, 74 (2013).

[38] Y. Zhou, J. Park, J. Shi, M. Chhowalla, H. Park, D. A. Weitz, and S. Ramanathan, Control of emergent properties at a correlated oxide interface with graphene, Nano Lett. **15**, 1627 (2015).

[39] R. Lopez, T. E. Haynes, L. A. Boatner, L. C. Feldman, and R. F. Haglund, Size effects in the structural phase transition of $VO_2$ nanoparticles, Phys. Rev. B **65**, 224113 (2002).

[40] J. Rensberg, Y. Zhou, S. Richter, C. Wan, S. Zhang, P. Schöppe, R. Schmidt-Grund, S. Ramanathan, F. Capasso, M. A. Kats, and C. Ronning, Epsilon-Near-Zero Substrate Engineering for Ultrathin-Film Perfect Absorbers, Phys. Rev. Appl. **8**, 014009 (2017).

[41] D. Karnopp, D. L. Margolis, and R. C. Rosenberg, *System Dynamics: Modeling, Simulation, and Control of Mechatronic Systems* (Wiley, Hoboken, New Jersey, 2012).

[42] Flir Research and Science, Use low-cost materials to increase target emissivity. Accessed online: www.flir.com (2015).

[43] A. Hendaoui, N. Émond, S. Dorval, M. Chaker, and E. Haddad, $VO_2$-based smart coatings with improved emittance-switching properties for an energy-efficient near room-temperature thermal control of spacecrafts, Sol. Energy Mater. Sol. Cells **117**, 494 (2013).

[44] T. G. Conway, R.-L. G. McClean, and G. W. Walker, Three color infrared camouflage system, US5077101A (1989).

[45] C. Chen, X. Yi, J. Zhang, and X. Zhao, Linear uncooled microbolometer array based on VOx thin films, Infrared Phys. Technol. **42**, 87 (2001).

[46] L. A. L. de Almeida, G. S. Deep, A. M. N. Lima, I. A. Khrebtov, V. G. Malyarov, and H. Neff, Modeling and performance of vanadium–oxide transition edge microbolometers, Appl. Phys. Lett. **85**, 3605 (2004).

[47] G. Wehmeyer, Y. Tomohide, C. Monachon, J. Wu, and C. Dames, Thermal diodes, regulators, and switches: Physical mechanisms and potential applications, Appl. Phys. Rev. **4**, 041304 (2017).